Monte Carlo simulation of the unwinding of cholesteric twist

Arunava Chatterjee and David H. Van Winkle
The Florida State University, Tallahassee, Florida 32306
(Received 15 July 1993)

The unwinding of cholesteric twist has been observed in liquid-crystalline DNA near the cholesteric-hexagonal columnar phase boundary. Disclination lines are seen to bound regions of different total twist. A Monte Carlo simulation, applying a molecular statistical model for the cholesteric phase, is used to model this unwinding and the disclination lines. We find disclination lines corresponding to edge χ lines. We also find evidence of $\lambda\tau$ pairs. These results are in agreement with expectations from phenomenological Landau–de Gennes theory and homotopy. Furthermore, the results obtained can be used to describe the terraced morphology observed in the DNA system.

PACS number(s): 61.30.Eb

I. INTRODUCTION

Cholesteric liquid crystals possess local nematic order and a macroscopic-twist axis perpendicular to the molecular long axis. This introduces a length scale for which translational symmetry in one direction is replaced by periodic symmetry (as indicated by the pitch p). The less symmetric cholesteric therefore allows for structures not found in ordinary nematics. As an example, consider the Cano wedge, where linearly increasing cell thickness introduces a discontinuous change in the observed pitch while local nematic order is preserved. The discontinuity appears as disclination lines. Recently, Van Winkle, Davidson, and Rill [1] observed a terraced morphology imposed by pretransitional divergence of pitch as the cholesteric approached the columnar phase in liquid-crystalline deoxyribonucleic acid (lcDNA). The morphology is similar to Grandjean planes seen in the Cano wedge and seen by Kelker in a cholesteric-nematic mixture with an imposed concentration gradient [2]. Unlike the mixture studied by Kelker, lcDNA is lyotropic and the twist unwinds with increasing concentration of DNA in solution. It was conjectured that the terraces were uniform planar textures of cholesteric DNA separated by disclination lines of strength $\frac{1}{2}$.

Using Monte Carlo (MC) methods, the terraces are simulated. Energetically costly disclination lines are found as expected from the phenomenological Landau–de Gennes theory. An estimate of defect energies with respect to the background is also obtained.

II. EXPERIMENTAL OBSERVATION

In aqueous solutions 50 nm long DNA fragments form lyotropic liquid crystals (lcDNA). This length is longer than typical thermotropic liquid crystals ($\sim$ 2.5 nm) and shorter than the Tobacco Mosaic virus (TMV) (=300 nm), which also forms a cholesteric phase in aqueous solution. The primarily electrostatic intermolecular interaction is different from the largely hard rod interactions exhibited by TMV and the coupled dipolar–van der Waals interaction which governs the behavior of thermotropics. The cholesteric phase of these DNA rods appears in coexistence with the isotropic phase for DNA concentrations between 150 mgDNA/ml and 220 mg/ml. It is fully cholesteric from 220 mg/ml to 400 mg/ml. Measurements of the cholesteric pitch show that it increases from $p = 2.2$ μm to 10 μm as the concentration increases from 270 mg/ml to 400 mg/ml [1]. At higher concentrations a hexagonal-columnar phase forms [3]. While morphological changes indicative of structural rearrangements occur at higher concentrations, the nature of the phase diagram is unclear.

Near the cholesteric-columnar phase boundary, planar cholesteric lcDNA textures in the presence of a concentration gradient exhibits unwinding of the twist wave vector $q = \frac{2\pi}{p}$. This behavior has been observed using optical microscopy in controlled drying experiments [1]. A DNA sample is placed between a coverslip and a slide. The system is then sealed except for a small aperture through which water is allowed to evaporate. The sample continues to dry, allowing formation of the high density phase. The unwinding of a cholesteric twist, for concentrations less than 400 mg/ml, is accompanied by the formation of interfaces which translate in the direction of decreasing

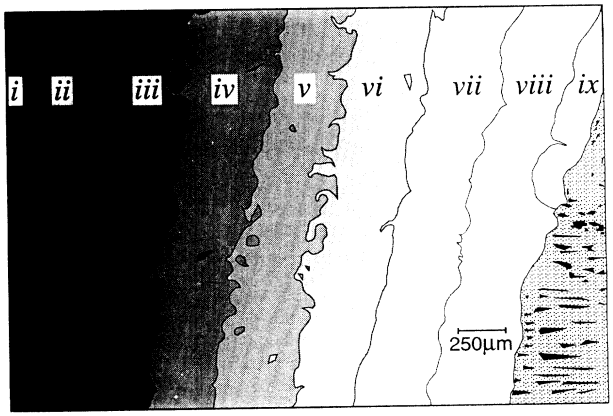

FIG. 1. Schematic of terraced morphology for an lcDNA sample under crossed polarizer and analyzer showing nearly evenly spaced regions of uniform twist.

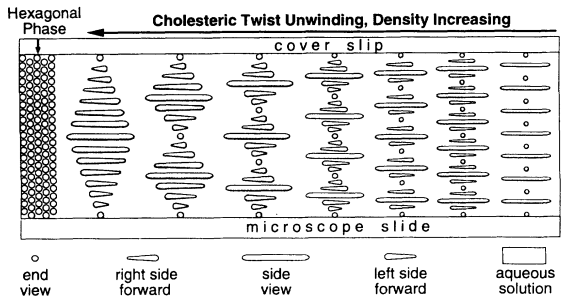

FIG. 2. Schematic representation of unwinding twist leading to the cholesteric to columnar transition.

DNA concentration. The translational velocity of the interface motion is extremely small with an upper bound of approximately 0.1 μm/s. It is therefore appropriate to treat the interfaces as quasiequilibrium structures. Optically, these interfaces appear as dark lines separating uniform birefringent regions. Each uniform domain exhibits distinct, concentration dependent shades of blue when observed between crossed polarizer and analyzer. Figure 1 shows a schematic illustrating these distinct regions. The schematic was obtained by scanning a photograph. The photograph itself is not shown since journal reproduction of the photo does not clearly display the boundaries between terraces that is evident in the original photomicrograph. Figure 2 is a representation of twist unwinding near the cholesteric-columnar boundary.

III. CHOLESTERIC PHENOMENOLOGY

A cholesteric liquid crystal is characterized by a twist. In the presence of physical boundaries, defects in uniform twist occur. The Landau–de Gennes continuum theory provides a basis for understanding cholesterics with defects.

Taking the z axis as the twist axis, the angular dependence of the molecular orientation for planar textures can be modeled as

$$\phi = qz + \phi_0. \tag{1}$$

Since the DNA binds strongly to glass surfaces, ϕ_0 is in general fixed, therefore the domains are characterized by quantized jumps in q (Fig. 2). That q is quantized for fixed boundaries can be shown by expressing the Frank free energy as a function of the polar and azimuthal angles. The associated Euler-Lagrange equations can be integrated numerically for planar textures to yield quantized wave number [4].

Since the terraces are stable over long times, they appear to be in equilibrium. Assuming that they are in equilibrium, homotopy argues that, in general, only disclination lines and point defects are stable [5–7]. In the absence of external fields, a simple argument offered by de Gennes shows that sheet disclinations and Bloch-like walls are unstable [8]. Given strong anchoring of the DNA at the slide and coverslip, the quantized wave number can only change discontinuously. A possibility that is consistent with homotopy and energy considerations (discussed below) is the formation of a single disclination line of half-integer strength between a region of $m\pi$ rotations and a region of $(m-1)\pi$ rotations. A succession of these line defects should arise as the cholesteric-columnar phase boundary is approached.

An estimate for the energy of disclination lines in nematics and cholesterics can be obtained by minimizing the distortion free energy [8, 9]. In the one constant approximation, the total distortion energy per unit length of line, ignoring core contributions, follows from integrating the local distortion energy,

$$F_d = \frac{n^2}{2}\frac{\kappa}{\rho^2}, \tag{2}$$

where n is the strength of the disclination, ρ is the radial distance from the line, and κ is an average elastic constant for distortion free energy. Thus, integrating over polar coordinates, the total distortion free energy between a core limit a and some distance ρ away from the disclination is

$$\mathcal{F} = \pi\kappa n^2 \ln\left(\frac{\rho}{a}\right). \tag{3}$$

By definition, this is also the line tension of the disclination. Using Eq. (3), with distances between defects ρ on the order of $10^4 a$, and $n = \frac{1}{2}$ disclinations, a rough estimate for the energy of defects in lcDNA terraces is 8κ.

A calculation for cholesterics that assumes small differences between elastic constants (a weakly "anisotropic" material) gives equivalent results to leading order with κ redefined as

$$\kappa = [(K_{11} + K_{33})K_{22}]^{\frac{1}{2}}, \tag{4}$$

where K_{11}, K_{22}, and K_{33} are splay, twist, and bend elastic constants, respectively [10]. This introduces a correction that depends on the intrinsic twist q_0 of the form

$$F_{\text{corr}} = \kappa C(q_0)\ln(2q_0 a). \tag{5}$$

The difference between splay and bend elastic constants is introduced through $C(q_0)$ with $C(q_0)$ given by

$$C(q_0) = \frac{\pi}{2}\left(\frac{K_{11} - K_{33}}{16(K_{11} + K_{33})}\right)^2 [13 - 2\cos(4q_0 h)], \tag{6}$$

where h is the height of the line along the cholesteric axis. For weak anisotropy, $C(q) \sim 10^{-3}$. Then for a pitch on the order of $10^3 a$, which is about the length scale in cholesteric DNA, the correction to the defect energy is less than 0.1κ.

In cholesterics, the simplest disclinations can be thought of as rotations of the director about one of three mutually perpendicular axes. A $2n\pi$ rotation (where n is an integer or half-integer) of the director about an axis parallel to the twist axis will generate a χ line. This rotation is identical to a dislocation given by Burger's vector of magnitude np, where p is the pitch, along the twist axis. Assuming the local director of the undistorted material is perpendicular to the twist axis, a $2n\pi$ rotation about an axis parallel to the director will generate a λ line, while a $2n\pi$ rotation about an axis perpendicular to

the director will generate a τ line.

For cholesterics, integer χ lines are not stable since these can be continuously transformed into structures without a core energy by some type of escape of the orientation field (e.g., into the third dimension). Unlike integer χ lines, half-integer χ lines cannot be transformed into structures without singular core while retaining the same strength. However, they can dissociate into $\lambda\tau$ pairs. In undissociated χ lines the molecules remain primarily perpendicular to the local twist axis. Integer lines have been observed, optically in the Cano wedge as thick threads. In the lcDNA terraces, only thin threads (characteristic of half-integer lines) were observed.

IV. SIMULATION

A. Microscopic model for cholesteric

The basic physics governing the interactions between rodlike DNA molecules in solution with 1:1 electrolyte is best described in terms of an ionic double layer theory as discussed for DNA by Schellman and Stitger [11, 12]. A discussion of some of the complications in understanding the interaction leading to twist and also to a change in twist with concentration is included in a previous paper [13]. For the purposes of these simulations, the details of the primarily screened Coulomb interaction are ignored and a nearest neighbor model expressing both the nematic alignment and the cholesteric twist is used. In a series of papers, van der Meer *et al.* [14–16] generalized a model by Goosens [17] for the cholesteric phase. Using a multipole expansion followed by second order perturbation theory they derived an interaction that is thermodynamically equivalent to

$$V = -J(\vec{a}_i \cdot \vec{a}_j)^2 - K(\vec{a}_i \cdot \vec{a}_j)[(\vec{a}_i \times \vec{a}_j) \cdot \hat{u}_{ij}]. \qquad (7)$$

The vector $\vec{a}_r$ represents the long axis of the rod and $\hat{u}_{rt}$ is the unit vector directed from the center of mass of rod r to rod t [15]. The values of J and K depend on the details of the interaction. This model was originally derived for thermotropics. Models for lyotropic chiral macromolecules have been derived using dispersion forces by Osipov and others [18–21]. These are equivalent to the interaction of Eq. (7) if shape effects and solvent properties are ignored.

The term involving J reduces the free energy by aligning the molecules. The term involving K reduces the free energy when there is a twist perpendicular to $\vec{u}_{rt}$ between neighboring molecules. Minimizing the average free energy density the preferred helical wave number $q = \frac{2\pi}{p_0}$, where p_0 is the preferred pitch, is found to be

$$q = \frac{K}{2J\langle r \rangle}, \qquad (8)$$

where $\langle r \rangle$ is the average center of mass separation. It should be noted that Eq. (7) leads to a one constant Frank elastic energy when solved in the mean field. In order to obtain differences between twist, bend, and splay elastic constants, additional terms (discussed below) must be included.

Using Eq. (7) to model the interaction yields a cholesteric with uniform twist. Since J and K are effectively constant this expression did not allow for the pitch to vary with the appropriate thermodynamic variable. Thus van der Meer and Vertogen [15] included fourth order terms from symmetry considerations

$$-L(\vec{a}_i \cdot \vec{a}_j)^4 + M(\vec{a}_i \cdot \vec{a}_j)^3[(\vec{a}_i \times \vec{a}_j) \cdot \hat{u}_{ij}]. \qquad (9)$$

Experimental evidence requires that $L \sim J$ and that $M \sim K$ while series convergence requires $L \ll J$ and $M \ll K$. Thus those parameters must be understood as purely phenomenological in order to use this fourth order interaction. Minimizing the average free energy density for this interaction, the helical wave number q can be shown to be

$$q = \frac{1}{\langle r \rangle}\left[\frac{(7K - 3M) - 4Mx^2}{(14J + 12L) + 16Lx^2}\right], \qquad (10)$$

where $x = \frac{\langle P_4 \rangle}{\langle P_2 \rangle}$ is the ratio of the thermally averaged fourth and second Legendre polynomials. The introduction of these higher order terms leads to differences between twist, bend, and splay elastic constants through quantities that depend on the relative values of the interaction constants as well as $\frac{\langle P_4 \rangle}{\langle P_2 \rangle}$ [15].

B. Monte Carlo

A number of researchers have used Monte Carlo techniques to study liquid-crystalline systems. Stroobants *et al.* have used hard core repulsion among spherocylinders to obtain nematic, smectic, hexagonal, and crystalline phases [22]. Numerous simulations using the Lebwohl-Lasher interaction have been conducted to study the isotropic to nematic transition [23]. Recently, Monte Carlo simulations have been used to study disclination cores in hard rods [24]. These simulations have verified earlier mean-field results [25] as well as indicated the existence of a microscopically escaped structure.

A review of Monte Carlo methods can be found in a collection of books and articles by Binder [26]. The topic of Monte Carlo simulations as applied to liquid-crystalline systems has been discussed by Zannoni [27] and Frenkel [28].

The results reported here were obtained using simulated annealing. In addition to the standard Metropolis algorithm and a uniform random number generator, a cooling parameter was used to accelerate convergence. A description of this procedure can be found in a series of papers by Kirkpatrick [29]. A series of Monte Carlo simulations were performed to model defects in cholesterics using modifications of Eq. (7). The use of simulated annealing in general improved convergence times and led to well defined cholesteric structures.

C. Calculation

The MC simulation employed a two dimensional lattice of rods with centers of mass fixed at the $L_z \times L_x$ lattice sites to represent a cholesteric liquid crystal. The axis parallel to the twist axis was chosen as the z axis while

an axis perpendicular to the twist was chosen as the x axis. Experimentally, the molecular alignment is planar at the glass surfaces and therefore perpendicular to the z axis. For this geometry, the interaction [Eq. (7)] can be cast in terms of a single angle $\delta\phi_{ij} = \phi_i - \phi_j$ and takes the form

$$E_{ij} = -J\cos^2(\delta\phi_{ij}) + K\cos(\delta\phi_{ij})\sin(\delta\phi_{ij})u_{ijz}. \quad (11)$$

Since strong anchoring of the DNA on the glass is assumed [30], rod orientations at upper and lower boundaries were usually fixed to $\phi(z=0) = \phi(z=L_z) = 0$.

For this interaction, since the coefficients are treated phenomenologically, the ratio $R = \frac{J}{K}$ is the only meaningful parameter. Hence the interaction was recast in terms of R as

$$\frac{E_{ij}}{K} = -R\cos^2(\delta\phi_{ij}) + \cos(\delta\phi_{ij})\sin(\delta\phi_{ij})u_{ijz}\,. \quad (12)$$

The range of values for R is lattice size dependent. The interaction $\frac{E_{ij}}{K}$ used for the simulation was in general normalized by the number of nearest neighbors used. Physically, the value chosen for R sets the preferred twist between neighboring molecules. The preferred twist is that $\delta\phi_{ij} = \delta\phi_p$, which is found by minimizing the orientational free energy.

The cooling parameter was varied between upper bounds of 100, 10, and 1 and lower bounds of 0.1, 0.001, 1×10^{-5}, and 1×10^{-7}. The freezing value of the cooling parameter was found to be 0.017 ± 0.005. In most simulations the cooling parameter was lowered exponentially as a function of the number of iterations from 1.0 to 0.001. The number of lattice configurations (passes) attempted for each value of the cooling parameter varied between 500 and 1000. Sampling was done every five passes and a correlation function comparing current values of ϕ on the lattice with those of the previous sampling was used to monitor statistical independence of samples [33].

Simulations were conducted on IBM and Silicon Graphics Personal Iris workstation computers using 20×20, 20×40, 50×50, 50×100, and 100×100 site lattices. The configuration space was viewed using Personal Iris graphics routines. A dithering algorithm which uses linear interpolation between lattice sites was used to establish a two-tone shaded image of the configuration space. Orientation parallel to the x axis was assigned the color black while orientation perpendicular to the plane of the lattice was assigned the color red. The resulting image was used to acertain the type of defects formed. Figure 3 shows a black and white postscript rendition of one such image, where red has been replaced with white.

D. Results

Various simulations were attempted to model the terraced structure shown in Fig. 1. The disclination lines seen in the experiment appear to be regularly spaced and of strength $\frac{1}{2}$. The initial goal of the simulation was to develop a better understanding of the microscopic interaction giving rise to the unwinding of twist prior to the formation of the columnar phase and to model this unwinding via a balance of the intermolecular forces and the boundary conditions. It was found that building a simple spatial gradient into the phenomenological energy was not sufficient to accurately describe the experimentally observed stability of defect position and spacing. Thus the goals for the project evolved into developing a model which yielded, for fixed boundary conditions, spatially separated, positionally stable disclination lines between cholesteric regions of different total pitch. With this evolution of goals, it was found that the functional form used for the variable R determined the important physics of the problem. Hence the results are separated into three sections based on the choice of this functional form.

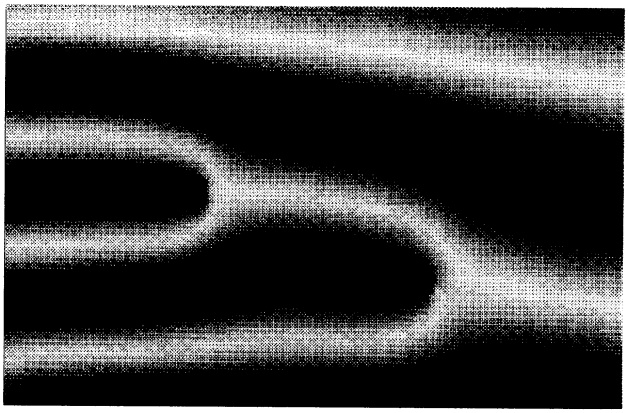

FIG. 3. An $m = 4$ to $m = 2$ unwinding showing two edge χ line disclinations on a 50×100 lattice. The image is a postscript rendition of a dithered color image generated using Silicon Graphics Personal Iris graphics routines.

Considering the lattice sizes used, finite size effects may be important. However, the observed textures were in qualitative agreement with expectations from the phenomenological Landau–de Gennes theory and are consistent with experimental observations. Thus finite size effects, if significant, did not give rise to unphysical results.

1. Constant R

The Monte Carlo algorithm was first employed using the interaction from Eq. (12), with constant R throughout the lattice. Fully periodic boundary conditions (in both x and z) were used to obtain a uniform constant twist throughout the lattice. The observed twist was determined both by the size of the lattice and by the value of R. Periodic boundary conditions in z are equivalent to putting the lattice on a torus and thus require that the molecular orientation twists through a quantized number of π rotations from $z = 0$ to $z = L_z$. The choice of R selects the relative azimuthal orientation difference between nearest neighbors in the z direction, $\delta\phi_p$, for which the orientational energy is a minimum. Thus the number of π rotations of the director which occur from $z = 0$ to $z = L_z$ is the integer closest to $L_z\frac{\delta\phi_p}{\pi}$. This is the manifestation of Eq. (1) representing the quantization of the twist wave vector $q = \frac{m\pi}{L_z}$ in the z direction.

Since the orientation of DNA fragments on glass sur-

faces is fixed by the anchoring conditions, a more realistic simulation would fix the top and bottom boundaries. The orientation was fixed at $z = 0$ and at $z = L_z$ (z boundaries) to $\phi = 0$. Periodic boundary conditions were maintained in the x direction. Again, the total change in orientation along the z direction was $\phi = qz$ with $q = \frac{m\pi}{L_z}$, but the orientation everywhere was determined by the boundary conditions.

Using these fixed boundaries, R was parametrized to find the range over which a particular total twist was stable. For example, on a 50×50 lattice a choice of $1.375 < R < 1.625$ yielded a structure with a 5π rotation of the molecular long axis. R determines the energetically most favorable angle between nearest neighbors independent of lattice size. Thus for simulations on different lattices, R must scale with the inverse lattice size to obtain the same number of rotations. This scaling is observed. For $50 \times L_x$ and $100 \times L_x$ lattices the range of values for R and corresponding twists were explored using a a step size of $\Delta R = 0.125$. A comparison of R as obtained from the mean-field result of Eq. (8) and those obtained for simulations using fixed z boundaries are shown for different lattice sizes for the case of $q = \frac{4\pi}{L_z}$ is as follows.

$q = \frac{4\pi}{L_z}$

Lattice size	Mean-field R	Simulation R
20×40	0.79	< 1.0
50×100	1.99	$1.5 < R < 2.125$
100×100	3.98	$3.75 < R < 4.125$

Simulations on a 50×50 lattice with $\Delta R = 0.125$ was used to obtain an estimate of valid R values for different twist. These values were compared with mean-field results. In the table below, n equals the number of π rotations.

n	Mean-field R	Simulation R
5	1.59	$1.375 < R < 1.625$
4	1.99	$1.5 < R < 2.125$
3	2.65	$2.0 < R < 2.875$
2	3.98	$2.75 < R < 5.25$

A few simulations were performed with other boundary values (with the difference in angle between top and bottom surfaces ϕ_0 as large as $\frac{\pi}{2}$) to check for stability and edge effects. These simulations resulted in a total twist of $\phi = m\pi + \phi_0$, exactly the form of Eq. (1).

The first attempts to simulate stable disclination structures were to fix the molecular orientations at the $x = 0$ and the $x = L_x$ boundaries with different twist wave vectors while keeping R constant. For example, $q = \frac{5\pi}{L_z}$ was chosen at $x = 0$ while $q = \frac{4\pi}{L_z}$ was chosen at $x = L_x$. The resulting simulations yielded 4π or 5π rotations (depending on the choice of R) everywhere except very close to the $x = 0$ or $x = L_x$ boundaries, where a disclination was pinned. To test further whether boundary conditions or the intermolecular interaction dominated the morphology, the boundaries were set to $q = m\pi$ rotations while an R was chosen which minimized the free energy for, as an example, $(m-2)\pi$ rotations. Distortions in a uniform twist structure were observed only very close to the x boundaries, while in the bulk $(m-2)\pi$ rotations formed. This implied that (i) the choice of R is the primary determinant of the resulting twist and (ii) the penetration depth associated with surface alignment was at most a few lattice sites for this nearest neighbor interaction. It was therefore expected that if R were allowed to vary with position, simulations would yield uniform twist regions seperated by disclination lines.

2. *Linear R*

In order to simulate the physical terraced system in which there exists a horizontal concentration gradient, a corresponding gradient in R was imposed,

$$R(x) = \left[\frac{R(L_x) - R(0)}{L_x}\right] x + R(0) . \tag{13}$$

The boundary values of $R(x = 0)$ and $R(x = L_x)$ were chosen such that different twist wave vectors q were preferred at $x = 0$ and $x = L_x$, respectively. For example, R could be chosen such that the distortion free energy would be mimimized for $m\pi$ rotations at $x = 0$ and for $(m-1)\pi$ rotations at $x = L_x$. Correspondingly, the x boundaries were fixed with the appropriate q. As before, the z boundaries were fixed to $\phi = 0$.

Disclination lines away from the x boundaries were obtained using the basic interaction of Eq. (12) and the linear variation in R. However, these defects were found to be mobile in the sense that multiple simulations resulted in a distribution of locations for the disclination lines. This distribution was quantified by measuring the standard deviations of the x location of the disclination lines to be as large as 15% of L_x. Imposition of different twists at the boundaries and a linear variation of R was therefore insufficient to model spatially stable defects.

Since a disclination implies local symmetry breaking of the uniform phase, various attempts were made to restrict defect mobility by imposing a symmetry breaking term in the interaction. The fourth order terms of Eq. (9) were added to Eq. (12) since their presence would lead to a competition between P_2 and P_4, the second and fourth order, order parameters. Neither the stability of the defects nor their structure as significantly affected. Next, the fourth order terms were replaced by a molecular field of the form $\langle P_4(\delta\phi_{ij})\rangle$ (not including nearest neighbors). The inclusion of this term simulates a competition between order parameters as well as a net contribution from the remainder of the lattice. Again, no significant changes were found. These simulations revealed that the x dependence of the energy could not be accounted for by competition between order parameters. A more complicated spatial dependence of R was therefore necessary to account for the changes in the strain energy due to the concentration gradient. Further, while fourth order terms are necessary to account for differences between Frank elastic constants, the one constant approximation is implicitly assumed in using Eq. (7). These results indicated that even if changes in K_{11} and K_{22}, which can be expected far from the transition, were accounted for in the simulation, the defect structure and stability would not be substantially altered.

3. Series R

Physically, although the concentration is a linear function of x the orientational free energy is not. Within a terrace, corresponding to $m\pi$ rotations, there will exist one x location where $\delta\phi_p(x) = \delta\phi_{ij}$, which satisfies $m\pi$ rotations. For both smaller and larger x $\delta\phi_p$, will not equal $\delta\phi_{ij}$ and the orientational free energy will not be an absolute minimum. Additionally, the energy of an $m\pi$ region should increase as the $(m-1)\pi$ boundary is approached. In Fig. 1, as an example, this would mean that the energy should increase as region v is approached from region iv. This corresponds to the additional strain energy due to strong anchoring at the boundaries. As a result, the defect energy is given by the difference between the relative maximum and minimum in the strain energy near the defect. The defect position is therefore selected by the location of these extrema in the sample. In the simulation, the use of fixed boundary conditions alone does not define the locations of these extrema. A similar result is seen for the Ising model with an interface. The interface is found to be unstable unless a surface tension term is included in the interaction [31]. While a surface tension is not an appropriate description of the boundary between two regions of different twist, an analogous behavior appears in the spatial dependence of the strain energy. An appropriate term which casts the line tension of the disclination in terms of the strain energy between two neighboring regions of different twist is therefore introduced.

In order to account for the additional contribution from the strain, R must have the physics of the interfaces built into its spatial dependence. We do not attempt to derive the functional form for the strain from a microscopic perspective. Rather, we employ an ansatz that provides spatially stable defects for the purposes of the simulation. The following form uses a hyperbolic tangent in analogy with Fréedericks interfaces [32]:

$$R = R(0) + \sum_i \left(A_i\{1+\tanh[C(x)-C_i]\} - B_{i+1}\{1+\tanh[C(x)-(C_i+\delta)]\}\right), \quad (14)$$

where the quantity A_i should be approximately as large as the energy of the ith defect, B_{i+1} is an indication of the maximum strain contribution in the $(i+1)$th region $(B_{i+1} < A_i)$, $[C(x) - C_i]$ selects the location of the defect and the associated concentration, and δ indicates the width of the minimum established by the two hyperbolic tangents of Eq. (14). Figure 4(a) shows the energy as a function of position in x averaged over z. We note that other forms for the strain contribution are certainly possible, so long as the general behavior is preserved. The time dependence as seen in the experiments on slowly drying samples can also be included in this model by letting $C(x) \to C(x,t)$. Defects obtained from simulations using Eq. (13) provided an estimate for A_i in Eq. (14). A choice of $B_2 = \frac{A_1}{3}$ and $B_3 = \frac{A_2}{3} + 0.1$ was used to obtain the conformation shown in Fig. 3. In this manner, the defect's position is stabilized and the DNA terraces are reproduced. An $m = 4$ to $m = 2$ unwinding is shown in Fig. 3 with $A_i = 0.375$. The series is truncated to two terms.

A few simulations in which the molecular orientations were allowed to vary in three dimensions were also conducted. These showed that the influence of boundary conditions on the selection of twist persisted over a length varying from 5 to 15 lattice sites from the sides in 50×50 and 50×100 site simulations. In these systems, for distances larger than this length from the boundary, a

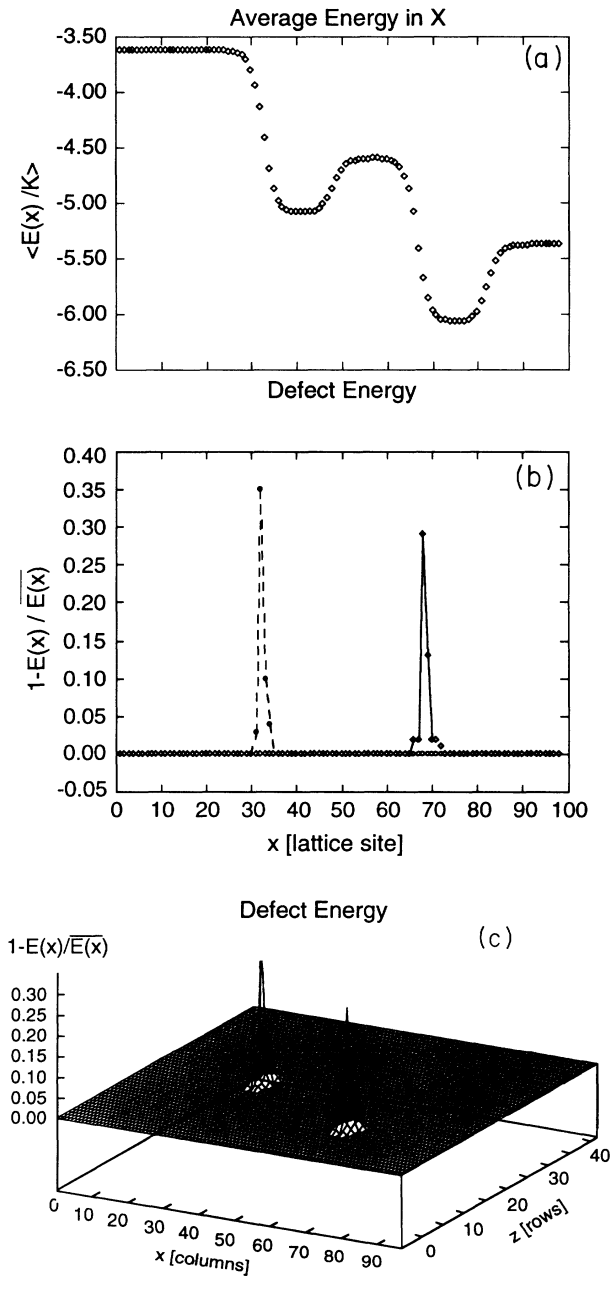

FIG. 4. (a) Energy as a function of position in x averaged over all rows. (b) Energy as a function of position in x showing two defects on a 50×100 lattice using series $R(A_i = 0.375, B_2 = \frac{A_1}{3}, B_3 = \frac{A_2}{3} + 0.1)$. (c) Energy as a function of position in x and z [same parameters as in (b)]. The average energy is calculated using a 1000 site sublattice not including the defects.

cholesteric conformation was not obtained. However, for the smaller systems mentioned ($20 \times L_x$), a well defined cholesteric was obtained. These simulations showed that alignment out of the cholesteric plane occurs near the defect core. While in some cases this out of plane alignment was consistent with χ lines [Fig. 5(a)], in other instances the out of plane alignment indicated $\lambda\tau$ pairs [Figs. 5(b) and 5(c)].

4. *Simulated defects*

Disclination lines were obtained in all of the simulations mentioned. In order to obtain the size, and energy cost associated with these structures, the energy deviations from the background was used. The structure of the defect was obtained using the dithered imaging mentioned in Sec. IV C, as well as the values of ϕ_i.

A defect width was defined for simulations involving Eq. (14). This was established as the number of lattice sites in x over which the energy per lattice site deviates from the background [Fig. 4(b)]. This deviation was calculated by dividing $\frac{E(x)}{K}$ for the row containing the defect by $\overline{\frac{E(x)}{K}}$ [where $\overline{E(x)}/K$ is an average over a sublattice that does not contain the defects] and subtracting the result from unity. Namely,

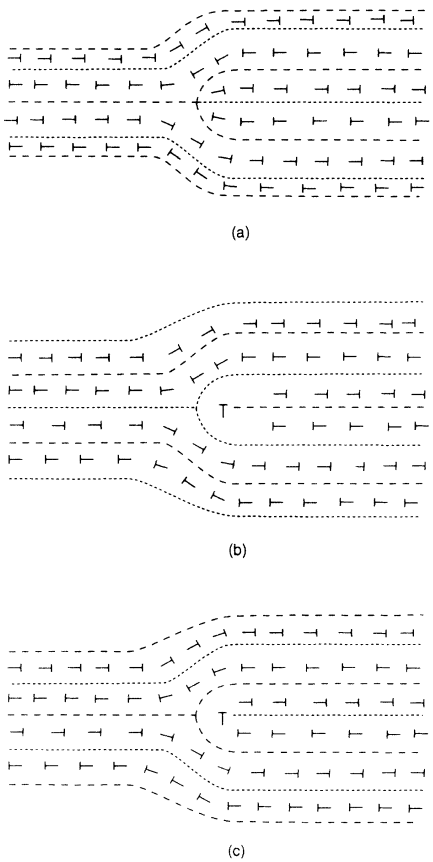

FIG. 5. (a) An edge χ line disclination showing the presence of an extra half-pitch region in a perfect cholesteric material. (b) A $\lambda^-\tau^+$ disclination pair. (c) A $\lambda^+\tau^-$ pair.

$$\delta\left(\frac{E(x)}{K}\right) = 1 - \frac{E(x)}{\overline{E(x)}}\,. \tag{15}$$

Figure 4(b) shows the energy per site, scaled according to Eq. (15), for a lattice row in a 50×100 lattice containing two defects. Figure 4(c) shows defect energies in a three dimensional format.

For 20×20 and 20×40 site simulations, defect widths were observed between three and four lattice sites, while for 50×50 and 50×100 site systems widths were observed between five and ten sites. By varying R as in Eq. (14), the increase in energy for the presence of a single defect was found to be between 20% and 40% above the background.

In order to compare the defect energy obtained from the MC simulations to that obtained from the continuum theory, the twist elastic constants must be resolved in terms of K and R. It has been shown that the interaction of Eq. (7), in the mean-field approach, is equivalent to the Frank elastic energy with a one-constant approximation [15]. The elastic constants are given by

$$K_{11} = K_{22} = K_{33} = \frac{1}{2}\left(\frac{N}{V}\langle P_2\rangle\right)^2 \int d\vec{r}_{ij} r^2{}_{ij} J(r_{ij})\,, \tag{16}$$

where N is the number of molecules in volume V. If K is assumed to be a constant, then $J = KR(r_{ijx})$. Further, away from the defect core $R(r_{ijx})$ changes weakly with r_{ijx}. Therefore, as a first approximation we take J to be a constant and evaluate the integral. Identifying κ of Eq. (2) with the elastic constants and using Eq. (15) to obtain the defect energy in terms of K leads to a form for the defect energy per unit length in terms of κ,

$$\mathcal{F} = \frac{4}{3\pi R\langle P_2\rangle^2}\kappa\left\langle\frac{E(x)}{K}\right\rangle\delta\left(\frac{E(x)}{K}\right)_{\max}\,, \tag{17}$$

where $\delta(\frac{E(x)}{K})_{\max}$ is the peak value of the defect energy. The resulting energy goes as $\frac{2.5}{R}\kappa$ for $\langle P_2\rangle^2 = 0.25$. This means that in general, the energy is considerably less than the continuum result for most thermotropics as well as lyotropics. The discrepancy results from the fact that the continuum theory assumes the defect interaction to be infinite in range while the MC simulation considers only nearest neighbors.

The disclination lines obtained from this model imply the collapse of a single half-pitch. These defects correspond to edge χ line disclinations [Fig. 5(a)] [34, 8]. In the Grandjean-Cano system, where the twist is required to change in a direction perpendicular to the twist axis due to a continuous change in cell thickness, the edge χ line is a likely structure [34, 8]. In the physical system, $\chi(\frac{1}{2})$ lines may dissociate into $\lambda\tau$ disclination pairs. However, this need not lead to a reduction in the defect energy, since the presence of a τ line introduces a finite core contribution. Results from simulations where both azimuthal and polar angles were varied imply that, for this model, $\lambda\tau$ pairs are also possible, since orientation out of the cholesteric plane in a manner consistent with $\lambda\tau$ pairs is observed. The extent of out of plane alignment

appears to depend on initial conditions. While in some cases χ lines are observed, in others the results indicate $\lambda^-\tau^+$ [Fig. 5(b)] or $\lambda^+\tau^-$ disclination pairs [Fig. 5(c)] [34,8]. Our results do not indicate a substantial reduction in the energy for out of plane alignment. However, since these structures were obtained only with small system sizes (20×20 and 20×40 lattices), where the coarseness of the lattice is of concern, conclusive remarks cannot be made at this point.

In conclusion, using the nearest neighbor interaction of Eq. (7) to model cholesteric defects, the disclination lines observed in lcDNA have been reproduced. We find that for lcDNA, the defect position is stabilized by the existence of a local minimum between strain energy barriers. The defects obtained from this model are $\chi(\frac{1}{2})$ lines, implying that in the physical system a single half-pitch region collapses. Allowing escape along the twist axis reveals that for small lattices ($20 \times L_x$), $\lambda\tau$ pairs are also possible. The simulations which yielded stable structures did not depend on the details of the lcDNA interaction. These results therefore also confirm previous interpretations of the structure of cholesterics in the Cano wedge and in cholesteric-nematic mixtures.

ACKNOWLEDGMENTS

We are indebted to J. Vinals and G. Frichter for advice on Monte Carlo simulations and A. Dalke for writing the Personal Iris graphics routine.

[1] D. H. Van Winkle, M. W. Davidson, and R. L. Rill, J. Chem. Phys. **97**, 5641 (1992).
[2] H. Kelker, Mol. Cryst. Liq. Cryst. **15**, 347 (1972).
[3] F. Livolant, A. M. Levelut, J. Doucet, and J. P. Benoit, Nature **339**, 724 (1989).
[4] D. W. Berreman and W. R. Heffner, J. Appl. Phys. **52**, 3032 (1981).
[5] G. Toulouse and M. Kleman, J. Phys. Lett. B **37**, L149 (1976).
[6] G. E. Volovik and V. P. Mineev, Zh. Eksp. Teor. Fiz. **72**, 2256 (1977) [Sov. Phys. JETP **45**, 1186 (1977)].
[7] L. Michel, Rev. Mod. Phys. **51**, 591 (1980).
[8] P. G. de Gennes, *The Physics of Liquid Crystals* (Oxford Press, London 1974).
[9] P. G. de Gennes, C. R. Acad. Sci. **266**, 571 (1968).
[10] C. Caroli and E. Dubois-Violette, Solid State Commun. **7**, 799 (1969).
[11] J. A. Schellman and D. Stitger, Biopolymers **16**, 1415 (1977).
[12] D. Stitger, Biopolymers **16**, 1435 (1977).
[13] D. H. Van Winkle, M. W. Davidson, W. X. Chen, and R. L. Rill, Macromolecules **23**, 4140 (1990).
[14] B. W. van der Meer, G. Vertogen, A. J. Dekker, and J. G. J. Ypma, J. Chem. Phys. **65**, 3935 (1976).
[15] B. W. van der Meer and G. Vertogen, in *The Molecular Physics of Liquid Crystals*, edited by G. R. Luckhurst, and G. W. Gray (Academic, New York, 1979).
[16] B. W. van der Meer and G. Vertogen, Phys. Lett. **59A**, 279 (1976).
[17] W. J. A. Goosens, Mol. Cryst. Liq. Cryst. **12**, 237 (1970).
[18] M. A. Osipov, Chem. Phys. **96**, 259 (1985).
[19] M. A. Osipov, Nuovo Cimento D **10**, 1249 (1988).
[20] T. V. Samulski and E. T. Samulski, J. Chem. Phys. **67**, 824 (1977).
[21] H. Imura and K. Okano, J. Chem. Phys. **58**, 2763 (1973).
[22] A. Stroobants, H. N. W. Lekkerkerker, and D. Frenkel, Phys. Rev. A **36**, 2929 (1987).
[23] For instance, see C. Chicolli, P. Pasini, and C. Zannoni, Physica A **148**, 298 (1988); S. Romano, Nuovo Cimento D **7**, 717 (1986); C. Zannoni, J. Chem. Phys. **84**, 424 (1986); U. Fabri and C. Zannoni, Mol. Phys. **58**, 763 (1986).
[24] S. D. Hudson and R. G. Larson, Phys. Rev. Lett. **70**, 2916 (1993).
[25] N. Schopohl and T. J. Sluckin, Phys. Rev. Lett. **59**, 2582 (1987).
[26] *Monte Carlo Methods in Statistical Physics*, edited by K. Binder (Springer-Verlag, Berlin, 1986).
[27] C. Zannoni, in *The Molecular Physics of Liquid Crystals*, edited by G. R. Luckhurst, and G. W. Gray (Academic, New York, 1979).
[28] D. Frenkel, Mol. Phys. **60**, 1 (1987).
[29] S. Kirkpatrick, J. Stat. Phys. **34**, 975 (1984).
[30] A. Klug, L. C. Lutter, and D. Rhodes, Cold Spring Harbor Symp. Quant. Biol. **47**, 285 (1983).
[31] D. Jasnow, Rep. Prog. Phys. **47**, 1435 (1983).
[32] F. Sagues and M. San Miguel, Phys. Rev. A **39**, 6567 (1989).
[33] D. Chandler, *Modern Statistical Mechanics* (Oxford University Press, Oxford, 1987).
[34] M. Kleman, in *Liquid Crystals and Plastic Crystals Vol.1*, edited by G. W. Gray and P. A. Windsor (Hortwood, Chichester, 1974).

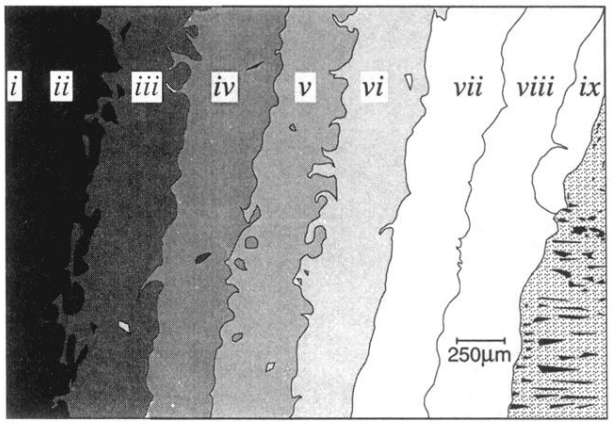

FIG. 1. Schematic of terraced morphology for an lcDNA sample under crossed polarizer and analyzer showing nearly evenly spaced regions of uniform twist.

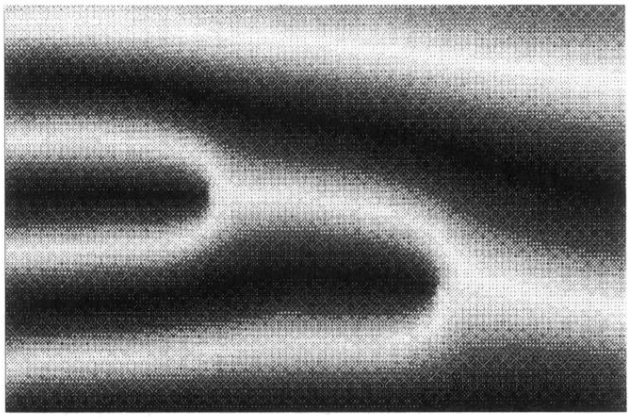

FIG. 3. An $m = 4$ to $m = 2$ unwinding showing two edge χ line disclinations on a 50×100 lattice. The image is a postscript rendition of a dithered color image generated using Silicon Graphics Personal Iris graphics routines.